Smart clothing with built-in soft sensing network for measuring temporal and spatial distribution of pressure under impact scenarios

*Fei Wang[1,2,9], Bo Zhu[2,3,9], Lin Shu[2,4,5], Ying Li[2,6], Xinghua Lai[7], Lingchen Ma[7], Peijun Ji[7], Qing Zhou[7], Tongxi Yu[8], Xiaoming Tao[2,6]**

[1]School of Textile Materials and Engineering, Wuyi University, Jiangmen, 529020, China

[2]School of Fashion and Textiles, The Hong Kong Polytechnic University, Hong Kong, 999077, China

[3]College of Professional and Continuing Education, The Hong Kong Polytechnic University, Hong Kong, 999077, China

[4]School of Future Technology, South China University of Technology, Guangzhou, 511422, China

[5]School of Electronic and Information Engineering, South China University of Technology, Guangzhou, 510640, China

[6]Research Institute for Intelligent Wearable Systems, The Hong Kong Polytechnic University, Hong Kong, 999077, China

[7]State Key Laboratory of Automotive Safety and Energy, Department of Automotive Engineering, Tsinghua University, Beijing, 100084, China

[8]Department of Mechanical and Aerospace Engineering, The Hong Kong University of Science and Technology, Hong Kong, 999077, China

[9]These authors contributed equally: Fei Wang, Bo Zhu

*Corresponding author, e-mail: xiao-ming.tao@polyu.edu.hk

Keywords: Smart clothing, pressure sensors, strain rate, in-situ measurement, impact tests, crash dummy

Abstract

Nowadays the need of protective devices in man-machine interface is increasing in the fields of traffic, sports, construction, and military, etc. Dynamic pressure sensing technology with a wide measuring range, high sensitivity, softness, and fast response is crucial for evaluation and optimization of the personal protective equipment under impact scenarios. However, current sensors hardly possess all the required characteristcs aforesaid. For the first time, this article reports the evaluation and application of an innovative soft pressure sensor with modulus of 2 MPa, maximum pressure of 8 MPa, and over 500-Hz frequency. A theoretical model, taking strain rate into consideration, is established to characterize the dynamic sensing behavior. Sensing network in the form of smart clothing is developed and trial used in a sled crash test, which is a standard approach to evaluate the safety of automobiles in collisions. The pressure distribution over the dummy's surface during the short crash process was acquired in real-time, and compared with numerical simulations. This work is important to the study of occupant injury and crashworthness design for vehicles, and it will benefit the automotive industry. With built-in sensing network, the smart clothing has promising applications in the pressure mapping of 3D flexible man-machine interface under impact scenarios.

1. Introduction

In the past decades, the emerging wearable technology[1] has led to extensive research on wearable pressure sensors for human health monitoring,[2] personal protective equipment,[3] etc. While the vast majority of them detect low pressures,[4] e.g., the pulse wave on the wrist at kPa level,[5] only scarce research on wearable sensors is conducted for high pressure measurement (at MPa level). However, measurement of dynamic loads and resistance to impacts on human body are of great significance for protective outfit. Nowadays, there is an increasing need of smart clothing for dynamic pressure measurement in the fields of transportation/traffic[6], sports[7], construction[8], and military (ballistic impacts[9]). In particular, the rapid motorization process has led to increasing traffic casualties,[10] including steering wheel injury, seat belt and airbag inflicted injuries from high dynamic pressure.[11] The injury severity is closely related with impact speed.[12] In contact sports, the impact force can be up to 3,427 N, with hand velocity of 9.14 m/s in Olympic Boxing.[13] In primary blast injuries, an impact pressure of 10 MPa for 0.1 ms can lead to a pulmonary survival rate of 1%.[14] Hence, the study of smart clothing with built-in soft pressure sensors will benefit those scenarios, by providing in-situ dynamic pressure information to help improve vehicle crashworthiness design, injury detection of human body, impact protection and energy absorption materials/structures. The crucial elements of such smart clothing are soft pressure sensors, which demand wide measuring range, high sensitivity, softness, and good dynamic properties. However, most of traditional sensors do not possess all the required characteristcs.

The prevailing standards and regulations for impact tests over the world are based on conventional technologies, involving force/displacement sensors[15] and accelerometers[6b]. These technologies have very good dynamic response and they have been successful in the measurement of impact force. However, as the conventional sensors are based on metal frames,[15] the rigidity of the structure hampers their application on the human body. Furthermore, the conventional sensors are usually installed at discrete locations in the system,[6b] making it difficult to map the curved surface of the human body as an array without interfering the mechanical flexibility.

Recently, many flexible and soft pressure sensors have been developed for human-machine interfaces,[2c, 16] but few can meet the requirement of flexibility/softness, pressure measuring range, and dynamic properties simultaneously (**Table S1**). On one hand, pressure measuring range is an essential requirement. Only sensors of measuring range at MPa level are applicable to quantify the real-time dynamic pressure.[17] On the other hand, softness or a low rigidity is also required so as to conform to the human body, which has a curved surface with the skin having Young's modulus of 30-70 kPa.[18] Besides, adequate softness is necessary to avoid secondary damage to human body during the interaction of impact. Previous flexible and soft pressure sensors typically work at 100 kPa level or below, e.g., piezoresistive sensors using reduced graphene oxide aerogel[19], carbon nanofibers[20] and printed conductive fabrics[21]. Capacitive sensors using carbon nanotubes[22] and silver nanowires[23] as active fillers for electrodes have reached a pressure measuring range at around 1 MPa. Sensors utilizing foams coated with graphene further reached 2 MPa.[24] Recently, a chitosan-poly (hydroxyethyl acrylamide) double-network hydrogel pressure sensor has shown a pressure range

up to 3.23 MPa.[25] However, the sensor exhibited poor linearity and large hysteresis even under quasi-static condition, which is due to the viscoelasticity of the gel material.

Another key requirement for impact testing is the dynamic properties of the sensors. All the above wearable sensing technologies have been developed under quasi-static conditions. The dynamic behavior of the sensor is equally important, but ignored in most studies. The rate-dependent property is a crucial factor for measuring the mechanical quantities under impact loadings at medium-to-high strain rate, as the shockwaves in nanoseconds to milliseconds may cause injury either in car accident, in concussion during playing football, or in blast injury.[26] Polymers especially elastomeric materials exhibit viscoelastic characteristics. The creeping and relaxation may behave differently when strain rate increases. For example, the constituent SU-8 materials demonstrated an elastic visco-plastic behavior with strain-rate hardening.[27] Besides, the electromechanical properties in high frequency range can be very disparate from those in low frequency and quasi-static conditions. In 2015, a light-weight mechanochromic pressure sensing material functional up to 17.6 – 20.4 MPa was developed with an exemplary characterization on the dynamic response of the inverse opals material.[27] The sensors are viable for dynamic impact tests. Unfortunately, they use change in reflective color to gauge magnitude and rate of force, excluding the impact duration. It will be challenging to conduct real-time measurement as the addition of color read-out device makes the sensing system complicated. Other sensors[15] with systematical characterization of dynamic behavior are typically rigid.

Among others, the FlexiForce™ force sensor developed by Tekscan (Tekscan, Inc., MA, USA) is widely used as pressure mapping devices. The sensor comprises two polyester sheets with row-column patterns of conductive coatings, which vary their electrical resistance inversely to the applied force.[21, 28] Despite the function of high-speed measurement with a wide range of 14 MPa, the force sensors suffer from a high cost of thousands of dollars, an indispensable software to manage pressure information and to compensate inherent drawbacks of the sensors including non-linearity and crosstalk effect, the inaccessibility to raw voltage data,[21] as well as the limited durability under shear forces.

In the present work, we conduct the dynamic evaluation of a soft pressure sensor (SPS) developed in our previous study, build up a theoretical model of strain rate effect on the sensing behavior, and fabricate a prototype of sensor network in the form of smart clothing for in-situ and real-time impact monitoring. Application of the smart clothing is demonstrated in sled crash tests. In order to study the safety performance of automobiles, collision test of a locomotive or vehicle carrying a dummy is a common technical means.[29] Traditional technologies, including force sensors, displacement sensors, accelerometers, strain gauges, and high-speed cameras, are currently used to capture the response of dummy during collisions, while there is no physical and wearable technology that could directly measure the pressure applied on the surface of dummy, except by numerical simulation. Besides, the pressure distribution applied by the protective device on the surface of dummy is another important factor to evaluate the occupant injury. Even if the measured results by conventional sensors fall in the safety range, there is still a possibility that the occupant may get injured by the seat belts if the pressure goes beyond a threshold. The smart clothing provides a real-time and in-situ measurement of the impact pressure applied on the dummy by the seat belts and seat cushion. The results show

reasonable agreement with numerical simulation, and more importantly, it reveals more information than the traditional measurement and numerical simulation. Although there is no standard about the pressure-aroused injury in the industry so far, the present sensing technology shows a potential supplement to the current test standard of automobile safety.

2. Characterization of SPS

2.1. Properties of SPS without encapsulation

The SPS was designed in our previous study.[17] It comprises a short cylinder made from polydimethylsiloxane (PDMS) and a fabric strain sensor (FSS) coated with carbon/silicone composite (**Figure 1A**). The FSS encloses the PDMS cylinder in the middle part. When being compressed, the cylinder expands laterally due to the large Poisson's ratio of PDMS, leading to a stretch on the FSS. According to the previous study,[17] the SPS with a 2 MPa modulus measures pressure up to 8 MPa with a high sensitivity of 100%/MPa, a good repeatability (lowest non-repeatability ±2.4% from 0.8 to 8 MPa), as well as a short response time (less than 0.1 ms).

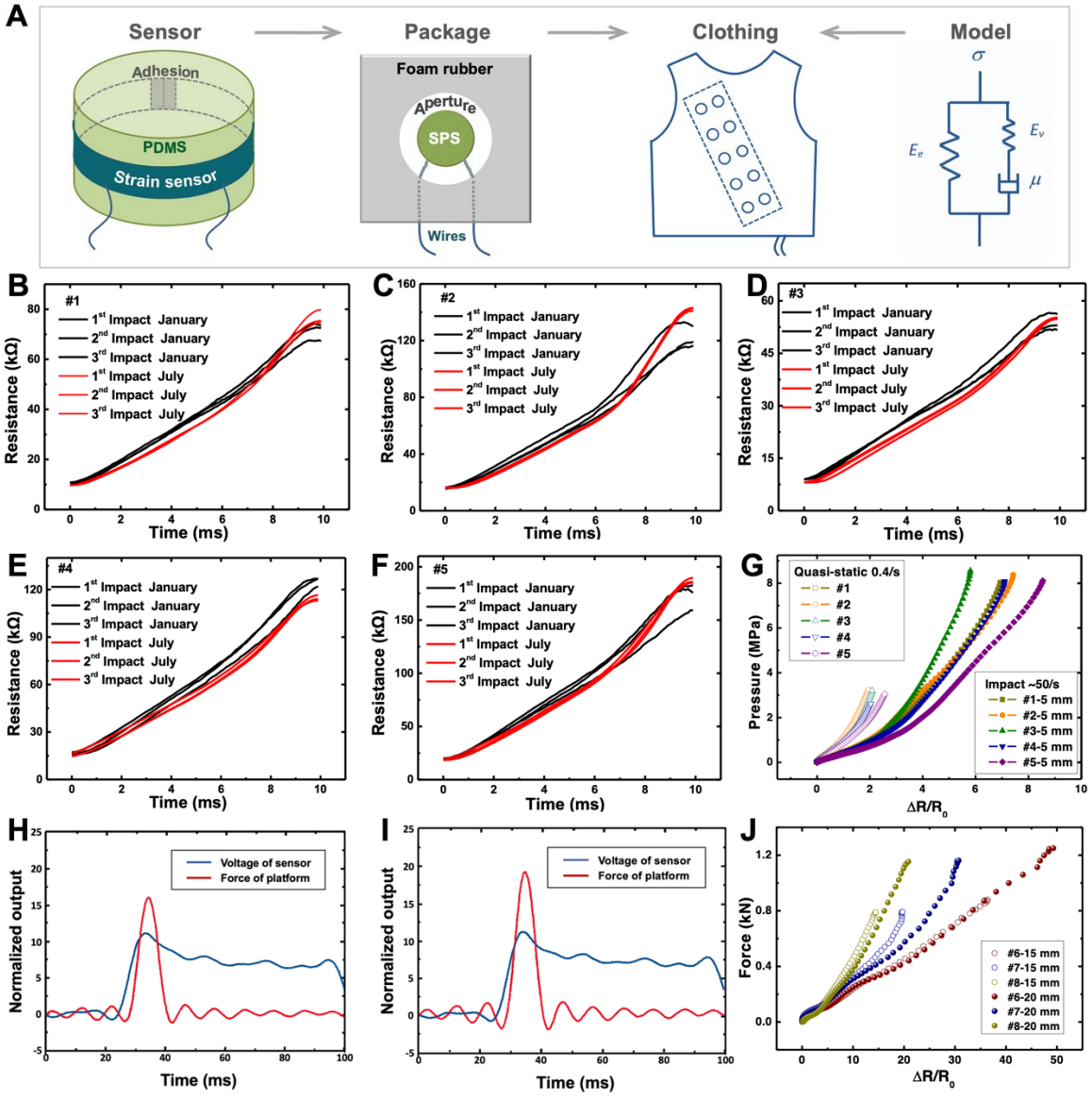

Figure 1. Schematic drawings and dynamic properties of SPS at various strain rate. (A) Schematics of SPS, package (top-view), and clothing. The last figure is a Generalized Maxwell model of viscoelasticity, which will be referred to in Section 3. (B) to (F) Resistance curves under dynamic loadings in two separate rounds with 6 months' time span. (G) Relative resistance change of five SPS samples under quasi-static and dynamic loadings; (H) to (I) Synchronized resistance and force signals of SPS sample in drop tower tests with height of (H) 15 mm; (I) 20 mm. (J) Relative resistance change of packaged SPS samples in drop tower tests with different heights, 15 mm and 20 mm.

Further, five SPS samples (#1-#5) were assessed in long-term stability (6 months) using the same experimental setup (drop tower test, **Figure S1A**) as in the previous study. Each sample first underwent one impact at a drop height of 8 mm as pretreatment and then four impacts at a drop height of 5 mm as testing. There was a 5 min interval between impacts. **Figure 1B-1F** gives the curves of six-month stability, where the black curves were obtained in January, and the red curves in July. When comparing the average of three peak resistance values with those acquired six months ago, the five SPS samples were found drifted by 7.7%, 16.9%, 2.6%, -8.6% and 8.3%, respectively. Besides the drop tower errors, the instability probably arose from the residual stress of fabric strain sensor produced during manufacturing process. The residual stress gradually relieved over 6 months, so that the consistencies or repeatability of three impacts in July were considerably superior to those in January. The improvement in repeatability reveals the necessity of annealing treatment in future SPS manufacturing.

2.2. Strain rate effect of SPS without encapsulation

Due to the viscoelastic nature of the conductive composite on the fabric and the PDMS, the SPS behaves differently under different loading speeds. In order to reveal the strain rate effect, the five samples of SPS were tested under quasi-static and medium-speed loads, using Instron and drop tower machine respectively, as represented by the curves in **Figure 1G**. In quasi-static compression, all the five samples were highly responsive to a pressure from 0 to around 3 MPa with their resistance doubled. The loading curves of the pressure sensors were smooth but nonlinear. In dynamic tests, all the five samples experienced a 5 mm drop test. The velocity of hammer approaching the SPS was 0.31 m/s. As a rough estimation, assuming the speed of load head decelerates uniformly in the compression process, and considering the thickness of package (~ 6 mm), the average strain rate during the impact is around 50 s^{-1}. The five SPS samples demonstrated notable strain rate effect (**Figure 1G**); that is, for a pressure of 3 MPa, relative resistance changes of pressure sensors under dynamic impact loading (~50 s^{-1}) were significantly greater than those in quasi-static compressions (0.4 s^{-1}).

2.3. Strain rate effect of SPS with encapsulation

To evaluate the performance of SPS with encapsulation, three more SPS samples (#6, #7, #8) were further packaged and tested using drop tower machine and DAQ. There was a five minutes interval between the consecutive drops. In the engineering field of automobiles, the typical strain rate of the dummy during car crash is 10 – 100 s^{-1}, and the pressure range is ~ 5 MPa. In order to cover the

ranges of pressure and strain rate, and to characterize the dynamic properties in situations close to the real crash, the drop height was selected as 15 mm and 20 mm for the samples of SPS with encapsulation. The relative resistance change vs. impact force under 15-mm and 20-mm drop height impact is shown in **Figure 1J**. Below the force of 0.6 kN, the resistance response was approximately linear. Above 0.6 kN, the slope of curves slightly decreased, which shared the same trend as in the quasi-static and 5-mm drop tests. For each sample, the resistance change under 20-mm drop height impact was a little larger than that under 15-mm drop height, revealing the effect of different strain rate. Within the linear range of 0.6 kN in force, for 30 mm × 30 mm package area, such a force caused a pressure of 0.67 MPa. However, due to the different nonlinear moduli of PDMS (**Figure 5C**) and packaging materials, PDMS cylinder in the center would probably cause a pressure of more than 5 MPa. As an approximate evaluation, despite large sample variations, the sensors exhibit measuring range of 0-5 MPa and a sensitivity up to 250%/MPa.

Figures 1H and **1I** show the curves of the measured force and the resistance varied with time under the drop height of 15 mm and 20 mm after 500 Hz filtering. It is seen that 20-mm drop height resulted in a higher impact force, leading to a greater resistance change, but the duration of impact is close to that under 15-mm, both being about 10 ms. Similarly, the speed of load head at the surface of sample is 0.54 m/s and 0.63 m/s, which corresponds to the average strain rate of 90 s^{-1} and 100 s^{-1}, respectively. Moreover, it is seen that the force signal starts to rise later than the resistance, which stems from the wave propagation through the sensor package and the drop tower. As the load head hits the surface of package, stress and strain waves arrive at the sensing element inside the package first, and then it travels down to the platform of the drop tower. Therefore, the start of force signal measured by the drop tower is a little later. This explanation can also be verified by the difference of time delay. As a well-known conclusion, higher strain rate on a viscoelastic system corresponds to higher modulus and faster wave speed, thus a shorter delay of the force signal. Under the 15-mm drop height, the instant of force rise is 3 ms later, while under the 20-mm drop height, the delay is about 2 ms.

As seen in **Figures 1I** and **1H**, the period of mechanical loading stage is detected as 7 ms under both the 15-mm and 20-mm drop heights, and the rise period of electrical resistance (of 80% Full-scale) is about 8 ms and 7.5 ms, respectively. This small difference of the resistance rise minus the force rise is also strain rate dependent. When the strain rate changes from 90 s^{-1} to 100 s^{-1}, faster wave speed in the viscoelastic system results in a shorter response time. As an underestimation, the response time under an ideal step loading (i.e., at infinite strain rate) would be shorter than 0.5 ms (= 7.5 ms – 7 ms); in other words, the frequency response of the sensor is above 500 Hz. However, a significant relaxation of resistance appeared after the impact load was unloaded, indicating that the sensor is not applicable to measure the unloading stage, but only suitable for measuring the loading stage of impact.

3. Theoretical model of strain rate effect

The pressure sensor consists of a conductive composite coated fabric as the sensing element and a PDMS cylinder as the receiver and transformer of pressure, both of which are based on soft polymers with different behavior under different loading speeds. Essentially, the input-output transition

undergoes mechanical pressure, deformation, and electrical resistance, so different mechanisms of mechanical and electrical behaviors may be involved. From a mathematical point of view, the relationships among the relevant quantities are all dependent on strain rate. In this regard, the theory of viscoelasticity is adopted to model the behavior of pressure sensor under dynamic loading, whilst it is noted that a few mathematical models have been previously proposed to quantify the strain rate effect.[30]

Considering the mechanical-electrical characteristics of the sensor under various strain rates, a generalized Maxwell model is more appropriate to represent the relation between mechanical pressure and resistance change. As sketched in **Figure 1A** (model), two elastic springs are connected with a dashpot in serial and parallel, respectively. Considering the serial connection of spring and dashpot, the stress-strain equations are given as

$$\begin{cases} \sigma_v = \mu\dot{\varepsilon}_\mu = E_v\varepsilon_v \\ \varepsilon_\mu + \varepsilon_v = \varepsilon \end{cases} \tag{1}$$

where σ_v is the stress, μ is the viscosity of dashpot, E_v is the modulus of spring, ε_μ and ε_v are the strains associated with the dashpot and spring, respectively, and ε is the total strain. Rearranging Equation (1) leads to

$$\begin{aligned} \mu\dot{\varepsilon}_\mu &= E_v(\varepsilon - \varepsilon_\mu) \\ \mu\dot{\varepsilon}_\mu + E_v\varepsilon_\mu &= E_v\varepsilon \end{aligned} \tag{2}$$

The general solution of the differential equation gives

$$\begin{aligned} \varepsilon_\mu(t) &= c(t)e^{-(E_v/\mu)t} \\ c(t) &= \int \frac{E_v\varepsilon(t)}{\mu e^{-(E_v/\mu)t}}\,dt \end{aligned} \tag{3}$$

where $c(t)$ is a time-dependent function about the total strain. Substituting Equation (3) into the stress expression in Equation (1),

$$\sigma_v(t) = E_v\varepsilon(t) - E_v e^{-(E_v/\mu)t}\int \frac{E_v\varepsilon(t)}{\mu e^{-(E_v/\mu)t}}\,dt \tag{4}$$

Finally, adding the spring in the parallel connection, the total stress of the generalized Maxwell model is expressed as

$$\sigma(t) = \sigma_e + \sigma_v = (E_e + E_v)\varepsilon(t) - \frac{E_v^2}{\mu}\frac{\int \varepsilon(t)e^{(E_v/\mu)t}dt}{e^{(E_v/\mu)t}} \tag{5}$$

It is found that given a fixed total stress, the total strain will increase with time and finally approaches a constant as well, which agrees with the electromechanical characteristics of the pressure sensor. If we define the pressure $p(t)$ as the input of the sensor whilst the relative resistance change $\lambda(t)$ as the output, then the pressure-resistance function takes an analogous form:

$$p(t) = (K_e + K_v)\lambda(t) - \frac{K_v^2}{K_\mu}\frac{\int \lambda(t) e^{(K_v/K_\mu)t} dt}{e^{(K_v/K_\mu)t}} \quad (6)$$

where K_e, K_v and K_μ are constants that quantify the effects of strain and strain-rate on the electromechanical behavior of the pressure sensor. Equation (6) provides a general expression of the SPS in mathematics, which will be further utilized for results analysis of sled crash test in Section 5.

4. Smart clothing and sled crash test

In order to monitor the dynamic pressure distribution applied on the body surface of a crash dummy during a standard sled crash test, a prototype of smart clothing integrated with SPS arrays was tailor-made for a three-point belted Hybrid III, a regulated anthropometric test device in automobile industry.[6a] The sensor-integrated dummy apparel and seat cushion were in-situ calibrated (details can be found in Supporting Information), and then used in standard sled crash test with in-situ and real-time pressure measurement beneath the seat belts and over the seat cushion.

The smart clothing took a style of vest and shorts (**Figure 2**) to simplify the apparel and the wearing process. Both the vest and shorts comprised front and back panels connected by Velcro® as shown in **Figures 2A** and **2B**. The two-panel design greatly facilitated the dressing on the dummy. In the front panel, there was a 2×5 sensing array which was both packaged and wired. The 2×5 sensor array covered an area of 40 mm × 250 mm, where sensor elements were 60 mm-equidistantly arranged in the length and 27 mm in the width. The SPS network was diagonally orientated along the location of the shoulder belt on the dummy, since in frontal crash test this area would be subject to greater pressure than other parts. Similarly, the shorts had its sensing network integrated in the horizontal direction, corresponding to the location of the lap belt. A prototype of smart clothing is depicted in **Figure 2**, where the numbers denote the sensors. There were 14 SPS elements distributed in the cushion according to the location of hips and thighs. Buckles on both sides of seat cushion were used to secure the cushion on the seat of sled.

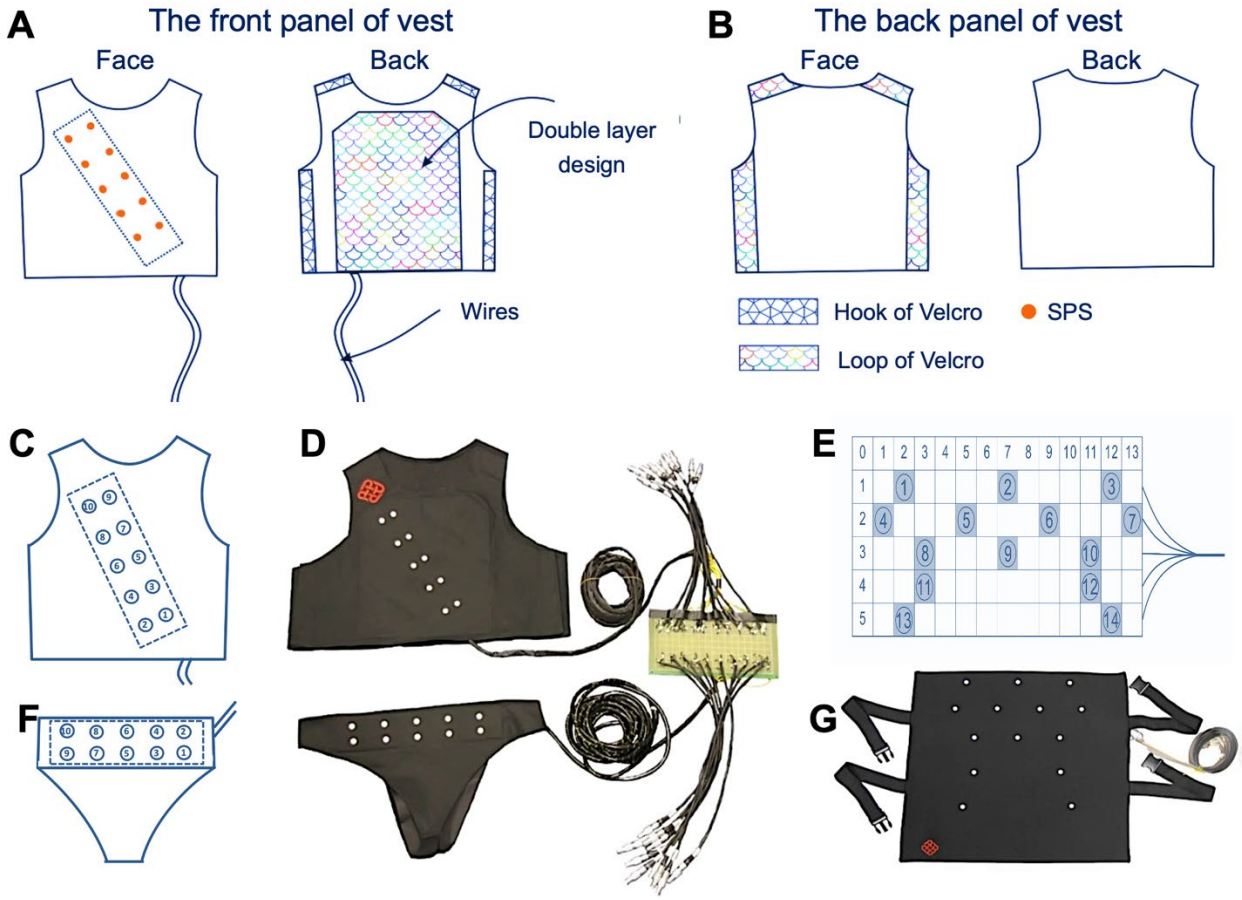

Figure 2. Design of smart clothing including vest and shorts for dummy, and cushion for seat. (A) Design of smart clothing, front panel of vest. (B) Back panel of vest. (C) Numbering of sensors on vest. (D) Picture of vest and short showing location of sensor array and cable connection to data acquisition system. The white dots mark the arrangement of sensor array. (E) to (F) Numbering of sensors on cushion and shorts (G) Picture of seat cushion.

The prototypes of dummy apparel and seat cushion were trial used by frontal sled crash tests in the Automobile Crash Test Laboratory, Department of Automotive Engineering, Tsinghua University, Beijing, China. The installations of apparel on the dummy, cushion on the seat, and the preparation of the sled are shown in **Figure 3**. The sled had a mass of 1,000 kg and the dummy had a mass of 75 kg. The crash pulse shaper was included to simulate frontal crash of practical car. An impact speed of 30 km/h was used. Dummy apparel was wire-connected to the KT device at a sampling rate of 10 kHz, and signals of seat cushion were wireless transmitted to a remote computer via Bluetooth at a sampling rate of 460 Hz. In addition to the prototype, acceleration of the sled and tensile force in the seat belts were both measured by conventional sensors and the KT device. Moreover, the crash process was also captured by a high-speed camera (**Video S1**), from which the details of dummy's movement can be clearly observed.

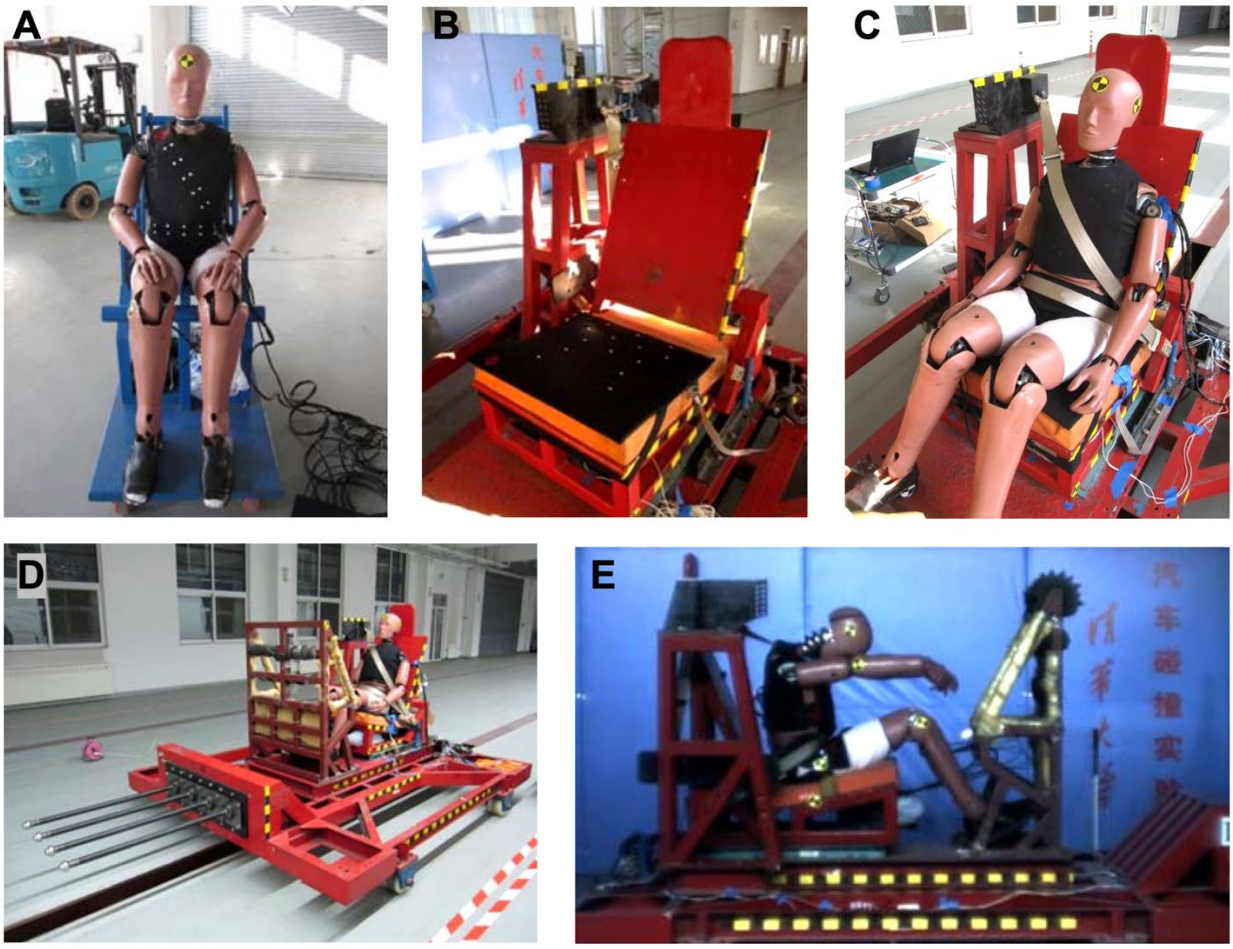

Figure 3. Photos of sled crash test. (A) The dummy wearing the smart clothing. (B) Smart seat cushion on the sled. (C) Dummy with safety belts fastened. (D) Sled with dummy from afar. (E) Snapshot in the video of crash test

5. Results of sled crash test

As theoretically modeled, the electrical-mechanical property of the sensor is dependent on strain rate; hence, the strain rates obtained from the in-situ calibration and sled crash test should be estimated and compared. Considering the drop height (~85 mm, Supporting Information) and the thickness of sensor array in the apparel (~10 mm), the average strain rate obtained from the in-situ calibration should be in the order of magnitude of ~100 s^{-1}. In the sled crash test, on the other hand, considering the duration of loading (~50 ms), the typical range of peak pressure (5~10 MPa), as well as the corresponding compressive strain on the sensor (~ 60%),[17] the average strain rate applied by the seat belt on the dummy is likely in the order of magnitude of ~10 s^{-1}. Therefore, the in-situ calibration results of sensor element must be compensated in terms of strain rate.

To simplify the analytical process, another reasonable approximation is adopted that during the loading stage, the resistance change is close to an exponential function of time as given by Equation (7), which agrees with the trend of the measured results:

$$\lambda(t) \approx e^{f(\dot{\varepsilon})t} \tag{7}$$

where the coefficient of exponent $f(\dot{\varepsilon})$ is a function of strain rate. Substituting it into Equation (6), we have

$$\frac{p(t)}{\lambda(t)} = K_e + K_v - \frac{K_v^2}{K_\mu}\frac{\int e^{f(\dot{\varepsilon})t} e^{(K_v/K_\mu)t} dt}{e^{f(\dot{\varepsilon})t} e^{(K_v/K_\mu)t}} = K_e + K_v - \frac{K_v^2/K_\mu}{f(\dot{\varepsilon}) + K_v/K_\mu} \tag{8}$$

Upon this assumption and simplification, a proportional relation exists between the pressure and resistance change, and the ratio is independent of time, only determined by sensor constants and strain rate, as indicated in Equation (8). From the test results at strain rate of ~1 s^{-1}, ~50 s^{-1} and ~100 s^{-1}, the effect of strain rate on the ratio $p/(\Delta R/R_0)$ is plotted in **Figure 4A**, while the values of $p/(\Delta R/R_0)$ is given in **Table 1**.

Table 1. Effects of strain rate in calibration and crash test

	In-situ calibration	Sled crash test
Average strain rate	~ 100 /s	~ 10 /s
Ratio of $p/(\Delta R/R_0)$	~ 0.3	~ 1.3

To compensate the strain rate effect, the $p/(\Delta R/R_0)$ curve obtained in the in-situ calibration is scaled down by a compensate factor of 0.23 (= 0.3/1.3) before being substituted into the measured results of sled crash test, as schematically shown in **Figure 4B**.

Finally, the pressure signals measured by each sensor element between the seat belts and dummy apparel were acquired, varying with time during the loading stage of crash process. **Figures 4G-4I** demonstrate the results of the vest, shorts, and cushion, respectively. During the crash process, the peak pressures at various locations of the belts and cushion are depicted in **Figures 4J** and **4K**.

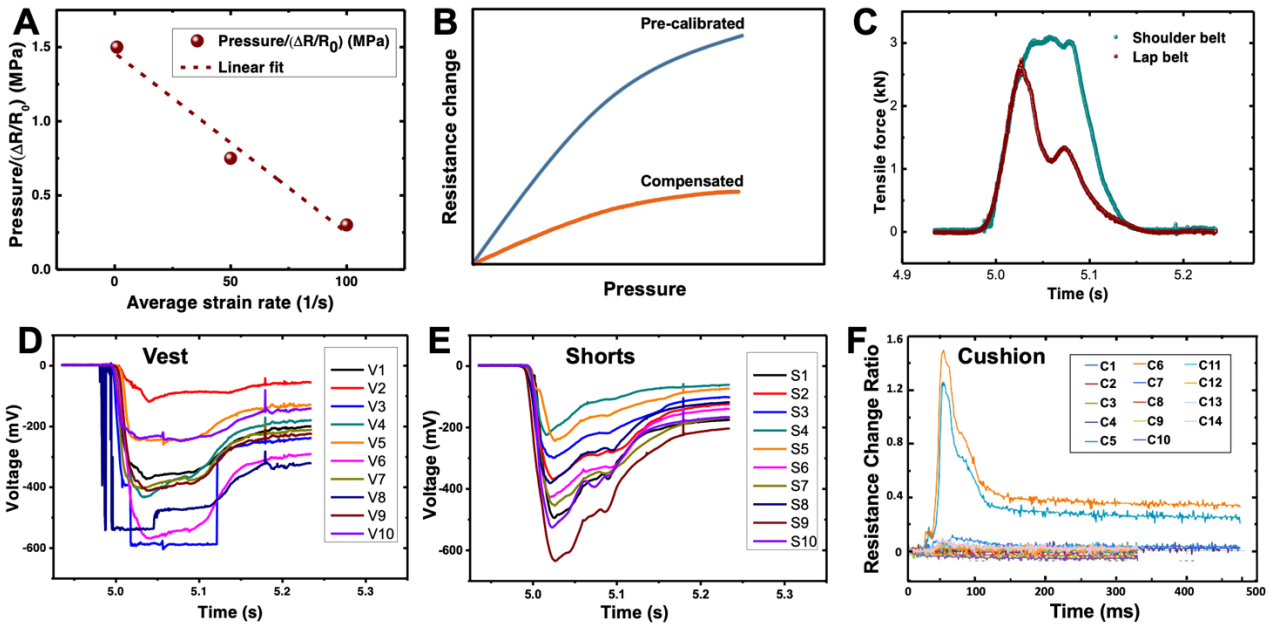

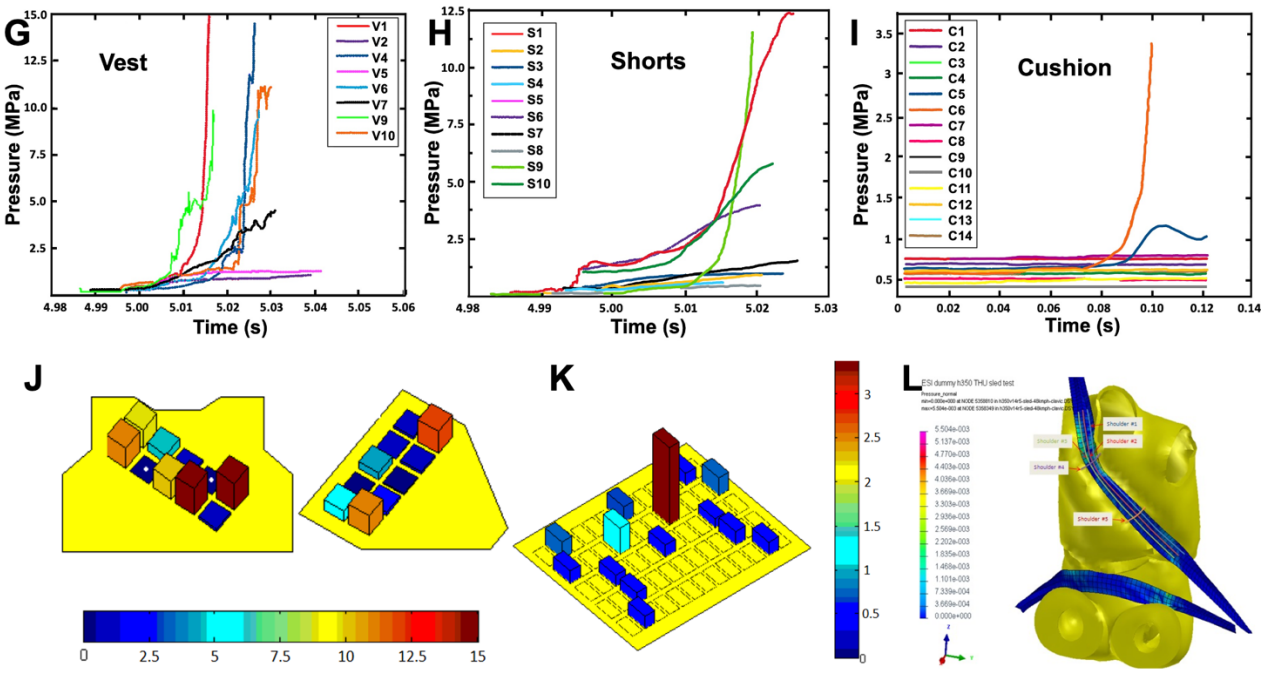

Figure 4. Measured results of sled crash test. (A) Effect of strain rate on the sensitivity of pressure sensor. (B) Schematic of compensation of calibrated results. (C) Tensile forces in the seat belts. (D) to (E) Voltage outputs of vest and shorts. (F) Relative resistance change of sensor array in the seat cushion. (G) to (I) Pressure variation during the sled crash test in vest, shorts and cushion, respectively. (J) to (K) Peak pressure values in the sled crash on dummy clothing and seat cushion (both color bars are in MPa). (L) Peak pressures in the numerical simulation results of the sled crash process.

The measured tensile force along the seat belts is plotted in **Figure 4C**, where the peak values in shoulder and lap belts are about 3,000 N and 2,500 N, respectively. The total duration of impact loading on the dummy body was about 190 ms, while the loading stage of shoulder and lap belts were both 50 ms. In account of that the human body injuries and safety performance are mainly relevant to the loading stage of an impact event, we will focus on the measurements within the first 50 ms of the impact duration.

The signals of sensors in the vest, shorts and cushion are plotted in **Figures 4D** to **4F**. As the sample of vest had already been overloaded several times in in-situ calibration, sensors V3 and V8 malfunctioned. Sensing elements in different locations had quite different magnitudes of output, which may be reasonably attributed to the non-uniform geometrical profile of dummy body and relative position of seat belts. **Figure 4F** shows the resistance outputs of the sensors in the cushion. It is clearly seen that sensors C5 and C6 gave greater signals, because they were located at the points with higher local pressure under dummy legs with sitting posture.

It is seen that the rising duration of the pressure varies from 10 ms to 30 ms at different locations, depending on the impact velocity and material properties of dummy. The distribution of pressure beneath the seat belt is non-uniform. Results of shoulder belt show that the upper part of the dummy's chest and the lower part of dummy's stomach underwent shorter impact durations and thus greater values of pressure, with an earlier onset of loading; whilst other parts of dummy' torso experienced

longer loading duration, smaller pressure, and later onset of loading. In the case of lap belt, the pressure on the two sides of dummy's abdomen was higher than that in the middle. Comparing the shoulder and lap belts, the peak pressure to dummy's torso was about 20% greater than that to dummy's abdomen. On the other hand, the mean value of the peak pressure at the 10 locations of shoulder belt was about 8 MPa, and that of lap belt was about 4 MPa.

On the cushion, most of the pressure concentrated at two sensor elements C5 and C6 (refer to **Figure 4I**). These pertained to the location of femur bones of the dummy, where most of the body weight was sustained. Moreover, the pressure difference between these two points indicates that the central axis of dummy did not align toward the front direction during the crash, but rotated leftward, resulting in asymmetric pressure distribution. The mean value of peak pressures on the cushion was about 1.5 MPa, much smaller than those beneath the seat belts.

It must be noted that, as some local pressures in the sled crash test was beyond the in-situ calibration range (~6 MPa), the corresponding pressure value was indirectly obtained by extension of the calibration curve. In this regard, the measured results over 6 MPa may contain greater errors.

6. Comparison with numerical simulations

In addition to experimental measurements, numerous numerical simulations have been widely conducted to analyze the impact process. [31] Most of the conditions set in the FEM are similar to our sled crash test, except that the impact velocity simulated usually is 48 km/h. **Figure 4L** illustrates the distribution of peak pressure on the surface of dummy beneath the seat belts. Refer to the locations of the sensor array, the peak pressure locates at the upper and lower parts in the vest, and at the two sides in the shorts, which agrees quite well with the measurement by the sensor array. On the other hand, numerical simulation results show that the mean value of peak pressures beneath the shoulder belt is greater than that beneath the lap belt, which is in accordance with the measurement as well. However, the value of peak pressure obtained from the numerical simulations are 5.5 MPa beneath the shoulder belt, and 3.7 MPa beneath the lap belt, which are much lower than the experimental measurement. The difference is mainly attributed to three factors. First, the material's parameters of the dummy set in the numerical simulation also contain approximations, and usually does not consider the increase of modulus of dummy under large compression; hence, the numerical simulation may underestimate the actual pressure during impact. Second, numerical simulation usually assumes smooth profile of dummy's geometry, homogeneous properties of dummy's material over the surface, and perfect contact and slide constrain between the seat belt and dummy; hence, geometrical deviation, local defects, or gap beneath the belts are not taken into consideration in the numerical simulation. Third, the sensor array is integrated with the sandwich foam in the apparel and attached with Velcro® on the surface of dummy, which causes difference from the naked dummy adopted in the numerical simulation. In particular, the PDMS of the sensor core is more rigid than the foam package and the panel of apparel, hence the sensor array would sustain a major portion of the total compressive force beneath the belts, resulting in a greater local pressure than the naked dummy adopted in numerical simulation.

Regarding the sled crash test, it is acceptable to have 50 measurements during the 50 ms of the loading stage, i.e., 250 Hz of frequency response. It is concluded that the pressure sensor, with frequency response above 500 Hz, fulfills the requirement of dynamic measurement under a medium strain rate of ~100 s^{-1}. By comparing with numerical simulation results, the measurement of the sensor array is reliable, and the accuracy is satisfied for engineering application.

7. Errors analysis

In the theoretical model of strain rate effect, the average strain rate in the Drop Tower and sled crash tests are adopted to compensate the strain rate effect. The error of the compensation is analyzed as below.

During the impact between the load head and the sensor, the strain rate of sensor is proportional to the velocity of the load head. Upon contact, the pressure over the surface increases, while the velocity decreases. The loading stage of impact is analogous to a quarter of mechanical vibration, with given mass, elastic modulus, initial velocity, and initial position, as sketched in **Figure 5A**.

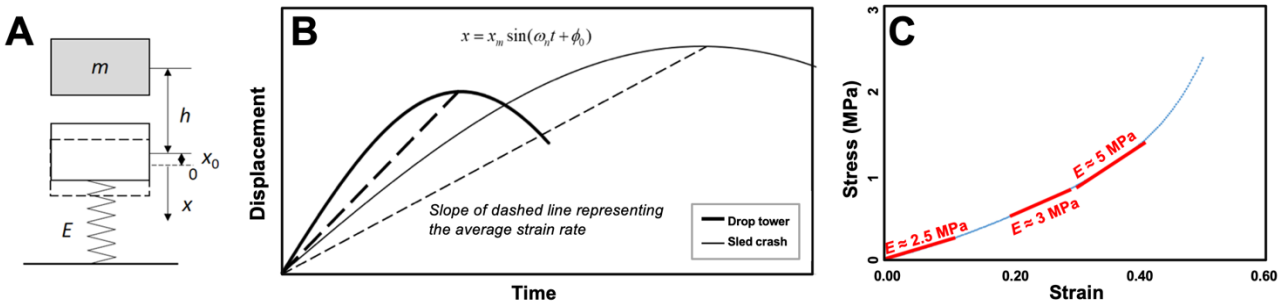

Figure 5. Error analysis of strain rate effect. (A) Impact of mass-spring system. (B) Schematic compression on the sensor vs. time during the impact process. (C) Compressive results of the sensor.

According to the classic theory of vibration, substituting the mass of load head m = 3.5 kg, drop height h = 85 mm, the modulus of sensor E = 2.13 MPa, the contact area A = 9 cm^2, and the initial thickness of sensor package l_0 = 10 mm, the angular frequency, initial position, initial velocity, and amplitude are evaluated in Equation (9).

$$\begin{aligned} \omega_n &= \sqrt{\frac{EA}{ml_0}} = 234 \text{ rad/s} \\ x_0 &= -\frac{mg}{EA/l_0} = 1.8\times10^{-4} \text{ m} \\ v_0 &= \sqrt{2gh} = 1.3 \text{ m/s} \\ x_m &= \sqrt{x_0^2 + \left(\frac{v_0}{\omega_n}\right)^2} = 5.6\times10^{-3} \text{ m} \\ \phi_0 &= \arctan\left(\frac{x_0\omega_n}{v_0}\right) = -0.032 \text{ rad} \end{aligned} \tag{9}$$

Accordingly, the function of displacement is expressed as a function of time in Equation (10).

$$x = x_m \sin(\omega_n t + \phi_0) = 0.0056\sin(234t) \tag{10}$$

Since the initial position is much smaller than the amplitude ($x_0 << x_m$), the initial phase can be neglected, and the displacement almost starts from the origin and undergoes a quarter of sine curve at the peak of maximum compression, as illustrated in **Figure 5B**.

A similar analysis can be applied to the impact between the seat belt and dummy in the sled crash test, and the displacement undergoes the similar curve of sine function, but in different amplitude and frequency. The average strain rate is represented by the slope of the dashed line connecting the origin and the peak point. It is admitted that the instantaneous strain rate, represented by the local slope on the curve, varies with time, whereas the ratio of instantaneous strain rates, at any moment of time, remains the same as the ratio of average strain rates. In this regard, the error of the strain rate effect is not attributed to the average, but attributed to the modulus of the sensor. Greater modulus corresponds to higher frequency and shorter period of vibration. Consequently, average strain rate would be higher. The ratio of strain rate is a square root of the ratio of modulus, as expressed in Equation (11). Therefore, if the modulus of sensor is a constant throughout the compression process, i.e., completely linear mechanical property, there would be no deviation of the average strain rate effect.

$$\frac{\varepsilon_2}{\varepsilon_1} = \sqrt{\frac{E_2}{E_1}} \tag{11}$$

Figure 5C shows the compressive test results of sensor. By approximate measurement, the modulus increases by 20% within the compressive strain of 0-0.3, and doubles at the strain about 0.4. Correlating with the pressure range, the deviation of the strain rate during the impact is roughly estimated as in **Table 2**. Results show that in the pressure range of 0-3 MPa, the error due to strain rate effect is about ±5%; in the range of 3-4 MPa, the error increases to ±20%; beyond 4 MPa, the error may be more significant because of the nonlinearity.

Table 2. Estimation of error range in different ranges of pressure measurement

Compressive strain	Pressure range	Increase of modulus	Deviation of strain rate	Error of strain rate effect
0-0.3	0-3 MPa	1.2	1.1	±5%
0.3-0.4	3-4 MPa	2	1.4	±20%

Secondly, because all the samples of individual sensor and sensor array are handmade in laboratory, there is a large sample variation up to 20%, which adds errors to the evaluation of the final results in the sled crash test. To reduce the variation, the relevant fabrication process must be better controlled, including pre- and post-treatment of the conductive composite, fabric coating, PDMS pillar, packaging with sandwich material, silicone adhesion on the flexible printed circuit board (FPCB), integration with apparel, etc.

Thirdly, the load duration of dynamic response test by the drop tower is not ideally zero, while the rise time of sensor output is in the same order of magnitude as the input dynamic load. Consequently, 500 Hz is an underestimation of the ideal frequency response of the sensor. More accurate result can be obtained by using better-controlled equipment with higher loading speed, e.g., Split Hopkinson pressure bar, hydraulic or pneumatic test machine.

In addition, the packaging material in the sensor array, the foam rubber, has a lower modulus and different dynamic property compared with the PDMS core. Consequently, the local pressure

measured by the sensor element would be higher than that without sensor. The packaging structure should be optimized and a material of more close property to the PDMS core is suggested in the future.

Last but not the least, stability and durability of the sensor is another factor of error. The test results show obvious resistance differences among the first and second dynamic loads, indicating that the first load already causes plastic deformation to the sensing composite of conductive fabric. This may be improved by pretreatment of the sensor after fabrication and addition of overload protection.

8. Conclusions

Based on the characterization of SPS under dynamic loadings, it is found in this study that the SPS meets all the key challenges of impact monitoring, including softness (2 MPa modulus), pressure measuring range (0–8 MPa), frequency response (> 500 Hz), and compensable strain rate effect, apart from the excellent regular sensor performances such as sensitivity, repeatability, stability, etc. Smart clothing imbedded with such sensor network demonstrated the capability of in-situ measurement of impact pressure distribution on the dummy body and the seat cushion during standard sled crash test. At the collision velocity of 30 km/h, the smart clothing showed the peak pressure of 6 MPa beneath the shoulder belt and 5 MPa beneath the lap belt; and the pressure on the two ends of the belts was noticeably higher than those in the center, which reasonably agrees with numerical simulation. The peak pressure on dummy's torso was 20% higher than that on abdomen. The experimental results of pressure distribution are in good accordance with those from numerical simulation, while the value of peak pressure is higher than the simulated results. In comparison, the measured results indicate the real case more accurately, as numerical simulation does not consider the defects of geometry and imperfection of material properties of dummy body.

This study was the first to use a smart clothing to acquire the in-situ and quantitative values of pressure distribution between the seat belts, seat cushion, and the dummy in a standard sled crash test. The strain rate-dependent sensing behavior is also theoretically modelled and compensated in the practical sled crash process. The error of the compensation for the strain rate effect is semi-quantitatively analyzed, showing different errors within different ranges of pressure. The SPS-integrated prototype provides a reliable means to get more mechanical information of dummy during the crash process, in addition to the measurement by conventional sensors, and to compare and verify the results of numerical simulation. The present research would benefit the industry of sensing technologies and smart clothing, as well as the field of contact sports, injury evaluation of human body, functional devices for impact protection and energy absorption.

9. Experimental Section

Drop tower test: A drop tower machine (King Design KD-3186-E, King Design Industrial Co., Ltd, Taiwan) was used (**Figure S1**), the falling mass of which was 5 kg. To record the electrical resistance of the SPS, a voltage divider and data acquisition equipment (DEWE-2600, Dewetron GmbH, Germany) were integrated. The load cell (Interface 1210 AF-1.5 kN, Interface Inc., USA) in the drop tower machine for impact force measurement was also connected to a data acquisition device. An excitation voltage of 10 V was applied to the voltage

divider, where an SPS and a reference resistor (56 kΩ) were connected in series. The voltage across the SPS was recorded by the data acquisition device at a sampling rate of 10 kHz. The electrical resistance of the FPS can be computed according to Equation (12), where *V* is the output voltage of the sensor.

$$R_{sen} = R_{ref} \times \frac{V}{10 - V} \tag{12}$$

Quasi-static test: A coupled electromechanical experimental setup was used, including Instron 5944 (Instron Corp., USA), an integrated versa channel, a voltage divider (excitation voltage is 10V),[32] and a computer for data display and storage. The compression force and the output voltage of the pressure sensors were measured simultaneously by Instron and the versa channel, respectively. A load was applied where the specimen was compressed to 2.75 mm for five cycles as pretreatment. After a recovery period of 2 min, the sensor was compressed to 2.5 mm for one more cycle. The loading speed of 60 mm/min was used for all the cycles. Electrical resistance of the sensor was then computed according to Equation (9), where *V* is the output voltage of the sensor. The reference resistor was 30.1 kΩ.

Package of SPS: In each package, the SPS glued at the center of a FPCB made from polyimide was surrounded by a sandwiching foam rubber material (5 mm in thickness, being equal to that of SPS). The material was ~ 0.4 MPa in compressive modulus and will be used in smart clothing. A round aperture of ϕ16 mm was made at the center of the foam rubber, so it doesn't restrain the SPS from deforming (**Figure 1-B**). After being wrapped by a black woven fabric, each final package was 30 mm × 30 mm × 6 mm in size (**Figure S1-B**).

Smart clothing system: The smart clothing consists of two major parts: a packaged pressure sensing network and a woven fabric sewn with Velcro®. Materials for the sensing network include customized PI-based FPCB, SPS elements, enameled copper wires, epoxy based electrically conductive adhesive (Eposolder 6510, United Adhesives Inc., USA), and packaging materials. The packaging materials are foam rubbers with thickness of 5mm and 2mm. Compressive modulus of the foam rubbers is around 0.4 MPa, while the initial modulus of soft pressure sensor is about 2.13 MPa. The effect of this difference is discussed in Sections 6 and 7. For the fabrication of smart vest, a pressure sensing network was first made. Ten SPS elements were glued to a PI-based FPCB using Tech-Bond adhesive and the wires of sensors were soldered onto the FPCB using conductive adhesives. The FPCB was then connected to a 1/4 bridge circuit board with LEMO connectors (high quality push-pull connector). A 2 mm thick layer of foam rubber was hot-pressed onto the backside of the FCB and further a punched middle layer (thickness 5 mm) as well as top layer (thickness 2 mm) were hot-pressed onto the FPCB. The pressure sensing network was finally integrated into the vest tailor-made for the dummy. Velcro® was sewn onto the vest in advance. Fabrication of the smart shorts and seat cushion followed a similar method. The dummy apparel system including the seat cushion was wire connected to a KT device (MINIDAU®System, Kayser-Threde GmbH, Munich, Germany), by LEMO connectors.

Supporting Information

Supporting Information is available from the Wiley Online Library or from the author.

Acknowledgements

This work is a part of a platform research project (ITP/007/10TP) primarily supported by the Innovation and Technology Fund of Innovation and Technology Commission, Hong Kong SAR. The authors would also like to acknowledge the support from the Endowed Professorship Scheme of The

Hong Kong Polytechnic University, and The Hong Kong Research Institute of Textiles and Apparel Limited, the sponsorship from Shenzhen NanHua Electronic Technology Corporation Ltd., Joint Sensor Instruments (Hong Kong) Ltd., and TAL Apparel Ltd., as well as a postgraduate scholarship from The Hong Kong Polytechnic University.

Conflict of Interest

The authors declare no conflict of interest.

Received: ((will be filled in by the editorial staff))

Revised: ((will be filled in by the editorial staff))

Published online: ((will be filled in by the editorial staff))

References

[1] a) W. Zeng, L. Shu, Q. Li, S. Chen, F. Wang, X.-M. Tao, *Advanced Materials* **2014**, 26, 5310; b) J. Shi, S. Liu, L. Zhang, B. Yang, L. Shu, Y. Yang, M. Ren, Y. Wang, J. Chen, W. Chen, Y. Chai, X. Tao, *Advanced Materials* **2020**, 32, 1901958.

[2] a) F. Wang, S. Liu, L. Shu, X.-M. Tao, *Carbon* **2017**, 121, 353; b) M. Cao, J. Su, S. Fan, H. Qiu, D. Su, L. Li, *Chemical Engineering Journal* **2021**, 406, 126777; c) T. Yang, D. Xie, Z. Li, H. Zhu, *Materials Science and Engineering: R: Reports* **2017**, 115, 1.

[3] L.-s. Zhang, J. Li, F. Wang, J.-d. Shi, W. Chen, X.-m. Tao, *Materials Science and Engineering: R: Reports* **2021**, 146, 100629.

[4] a) N. Luo, J. Zhang, X. Ding, Z. Zhou, Q. Zhang, Y.-T. Zhang, S.-C. Chen, J.-L. Hu, N. Zhao, *Advanced Materials Technologies* **2018**, 3, 1700222; b) S. Gong, W. Schwalb, Y. Wang, Y. Chen, Y. Tang, J. Si, B. Shirinzadeh, W. Cheng, *Nature Communications* **2014**, 5, 3132.

[5] a) X. Fan, Y. Huang, X. Ding, N. Luo, C. Li, N. Zhao, S.-C. Chen, *Adv. Funct. Mater.* **2018**, 28, 1805045; b) H. Park, Y. R. Jeong, J. Yun, S. Y. Hong, S. Jin, S.-J. Lee, G. Zi, J. S. Ha, *ACS Nano* **2015**, 9, 9974.

[6] a) P. Lesire, F. Leopold, X. Trosseille, H. Johannsen, P. Beillas, F. Alonzo, M.-C. Chevalier, DOI: https://doi.org/10.4271/2012-22-0010, The Stapp Association, 2012; b) G. J. Sequeira, R. Lugner, U. Jumar, T. Brandmeier, *J. Sens. Sens. Syst.* **2019**, 8, 19.

[7] a) T. Whyte, C. A. Stuart, A. Mallory, M. Ghajari, D. J. Plant, G. P. Siegmund, P. A. Cripton, *Journal of Biomechanical Engineering* **2019**, 141; b) N. Petrone, G. Candiotto, E. Marzella, F. Uriati, G. Carraro, M. Bäckström, A. Koptyug, *Journal of Science and Medicine in Sport* **2019**, 22, S78.

[8] a) C. Harris, *Journal of Forensic Nursing* **2013**, 9; b) R. A. Haslam, S. A. Hide, A. G. F. Gibb, D. E. Gyi, T. Pavitt, S. Atkinson, A. R. Duff, *Applied Ergonomics* **2005**, 36, 401.

[9] a) C. R. Bass, R. S. Salzar, S. R. Lucas, M. Davis, L. Donnellan, B. Folk, E. Sanderson, S. Waclawik, *International Journal of Occupational Safety and Ergonomics* **2006**, 12, 429; b) H. Liu, J. Kang, J. Chen, G. Li, X. Li, J. Wang, *International Journal of Medical Sciences* **2012**, 9, 655.

[10] G. Zhang, K. K. W. Yau, X. Zhang, Y. Li, *Accident Analysis & Prevention* **2016**, 87, 34.

[11] K. Kibayashi, R. Shimada, K.-i. Nakao, *IATSS Research* **2014**, 38, 71.

[12] C. Jurewicz, A. Sobhani, J. Woolley, J. Dutschke, B. Corben, *Transportation Research Procedia* **2016**, 14, 4247.

[13] T. J. Walilko, D. C. Viano, C. A. Bir, *Brit J Sport Med* **2005**, 39, 710.

[14] G. W. Wood, M. B. Panzer, J. K. Shridharani, K. A. Matthews, B. P. Capehart, B. S. Myers, C. R. Bass, *Injury Prev* **2013**, 19, 19.

[15] a) Y. Li, Z. Yang, G. Wang, C. Yang, *ISA Trans.* **2020**, 104, 382; b) H. A. Dinovitzer, A. Laronche, J. Albert, *IEEE Sensors Journal* **2019**, 19, 5670.

[16] F. He, X. You, W. Wang, T. Bai, G. Xue, M. Ye, *Small Methods* **2021**, 5, 2001041.

[17] F. Wang, B. Zhu, L. Shu, X. Tao, *Smart Materials and Structures* **2013**, 23, 015001.

[18] R. B. Groves, S. A. Coulman, J. C. Birchall, S. L. Evans, *Computer Methods in Biomechanics and Biomedical Engineering* **2012**, 15, 73.

[19] Z. Xiao, W. Zhou, N. Zhang, Q. Zhang, X. Xia, X. Gu, Y. Wang, S. Xie, *Small* **2019**, 15, 1804779.

[20] S. Peng, P. Blanloeuil, S. Wu, C. H. Wang, *Advanced Materials Interfaces* **2018**, 5, 1800403.

[21] I. Baldoli, M. Maselli, F. Cecchi, C. Laschi, *Smart Materials and Structures* **2017**, 26, 104011.

[22] D. J. Lipomi, M. Vosgueritchian, B. C. K. Tee, S. L. Hellstrom, J. A. Lee, C. H. Fox, Z. Bao, *Nature Nanotechnology* **2011**, 6, 788.

[23] S. Yao, Y. Zhu, *Nanoscale* **2014**, 6, 2345.

[24] a) Y. Pang, H. Tian, L. Tao, Y. Li, X. Wang, N. Deng, Y. Yang, T. L. Ren, *ACS applied materials & interfaces* **2016**, 8, 26458; b) X. Lü, T. Yu, F. Meng, W. Bao, *Advanced Materials Technologies* **2021**, 6, 2100248.

[25] Y. Yang, Y. Yang, Y. Cao, X. Wang, Y. Chen, H. Liu, Y. Gao, J. Wang, C. Liu, W. Wang, J.-K. Yu, D. Wu, *Chemical Engineering Journal* **2021**, 403, 126431.

[26] S. P. Broglio, J. J. Sosnoff, S. Shin, X. He, C. Alcaraz, J. Zimmerman, *Journal of athletic training* **2009**, 44, 342.
[27] Y. Cho, S. Y. Lee, L. Ellerthorpe, G. Feng, G. Lin, G. Wu, J. Yin, S. Yang, *Advanced Functional Materials* **2015**, 25, 6041.
[28] R. Ouckama, D. J. Pearsall, *Journal of Biomechanics* **2011**, 44, 904.
[29] P. Beillas, F. ALONZO, M.-C. CHEVALIER, P. LESIRE, F. LEOPOLD, H. JOHANNSEN, *Stapp Car Crash Journal* **2012**, 56, pp. 387.
[30] a) J. Wesseloo, A. T. Visser, E. Rust, *Geotextiles and Geomembranes* **2004**, 22, 273; b) T. K. Hight, J. F. Brandeau, *J. Biomech.* **1983**, 16, 445.
[31] a) D. Vangi, F. Begani, M.-S. Gulino, F. Spitzhüttl, *IFAC-PapersOnLine* **2018**, 51, 837; b) Y. A. Abdel-Nasser, *Alexandria Engineering Journal* **2013**, 52, 295.
[32] W. G. Tao XM, Wang YY and Zhang H. A method for manufacturing fabric strain sensors. US Patent Application No. 12/122,883, 19 May, 2008.

Xiaoming Tao is Chair Professor of Textile Technology and Director of Research Institute for Intelligent Wearable Systems at The Hong Kong Polytechnic University. She has a BEng in textile engineering and Ph.D. in textile physics. Prof. Tao is known internationally for her pioneering work on smart textiles and fiber-based electronics and photonics. She is a recipient of Honorary Fellowship of the Textile Institute, UK; Founder's Award from the Fiber Society of USA; and Guanghua Engineering Science and Technology Award by Chinses Academy of Engineering.

TOC

Title: Smart clothing with built-in soft sensing network for measuring temporal and spatial distribution of pressure under impact scenarios

Fei Wang[#], Bo Zhu[#], Lin Shu, Ying Li, Xinghua Lai, Lingchen Ma, Peijun Ji, Qing Zhou, Tongxi Yu and Xiaoming Tao[*]

For the first time, this research uses a smart clothing to acquire the in-situ and quantitative values of pressure distribution between the seat belts, seat cushion, and the dummy in a standard sled crash test. The smart clothing with soft pressure sensing network can be used in real-time pressure mapping of 3D flexible man-machine interface under impact scenarios.

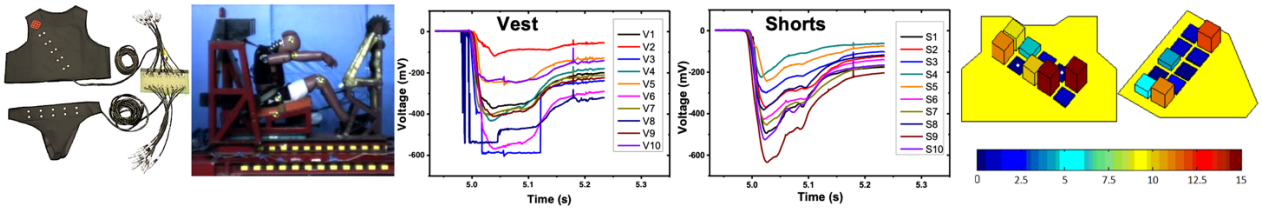

Supporting Information

Title: Smart clothing with built-in soft sensing network for measuring temporal and spatial distribution of pressure under impact scenarios

Fei Wang[#], Bo Zhu[#], Lin Shu, Ying Li, Xinghua Lai, Lingchen Ma, Peijun Ji, Qing Zhou, Tongxi Yu and Xiaoming Tao[*]

Supporting Experimental Section

In-situ calibration of prototype: The initial condition of the sensor is affected by the fabrication and packaging of the dummy apparel and seat cushion. In addition, due to the significant sample variation in the lab fabrication process, each sensor element in the array must be calibrated individually just before the sled crash test. As shown in **Figure S1-E**, a drop tower with 3.5 kg loading mass was used for the in-situ calibration under drop height of 85mm, with a contact area of 25 mm × 25 mm on each sensing element. An accelerometer was adhered on the loading head.

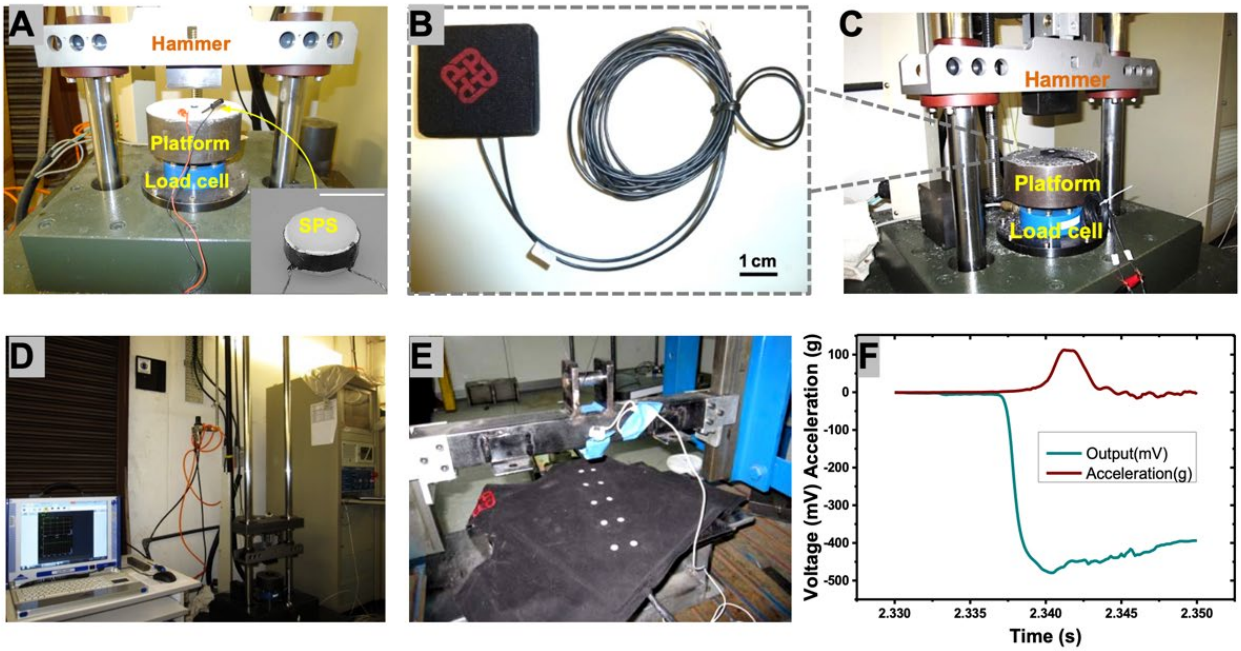

Figure S1. Drop tower test of single pressure sensors, single sensor package, and in-situ calibration of smart clothing. (A) Picture of drop tower test of bare SPS. Both the SPS and load cell were cable connected to the DEWE DAQ system. Inset is an SPS element, where the scale bar is 1 cm. (B) Picture of an encapsulated SPS with a logo of The polytechnic university printed on top. (C) SPS package under drop tower test. (D) SPS package under drop tower test including the DAQ system on the bottom left corner and the drop tower machine on the right. (E) Picture of in-situ calibration of smart clothing before sled crash test. (F) Typical results from calibration.

Both signals of the acceleration and resistance were acquired by the KT device. The output of sensor in KT is voltage via full bridge connection, and the relation between voltage output V and the relative resistance change is

$$\lambda = \frac{-1}{250/V + 0.5} \tag{S1}$$

Typical result obtained from the sensing elements is plotted in **Figure S1-F**. It is seen that the peak of acceleration occurs later than that of voltage, which is due to the same reason of stress wave propagation in the soft package and damping material as mentioned in Section 2.3.

Instead of resistance change, the voltage signals of the full bridge in the KT device are referred as the output of the sensor. The impact force and corresponding pressure can be calculated by the measured acceleration as

$$p = \frac{m(a+g)}{A} \tag{S2}$$

After correlating the starting and peak points of the two curves, the calibrated relations between the input pressure and the output voltage can be obtained for results analysis of the sled crash test.

The crash process captured by a high-speed camera:

Video S1 https://www.dropbox.com/s/gqo82jec38v8qit/

Table S1. Key parameters of typical wearable pressure sensors

Principle	Sensing Materials	Flexibility	Range (MPa)	Sensitivity (MPa^{-1})	Repeatability (%)	Response time (ms)	Ref.
Resistive	Carbon blacks(CB)/silicone	Soft	0-8	1.0	±2.4	0.1	[1]
Piezoresistive	Graphene	Soft	0-2	-0.9	-	-	[2]
Piezoresistive	Carbon nanofibers	Soft	0-0.002	-3 600	-	50	[3]
Resistive	Reduced graphene oxide (rGO) aerogel	Flexible	0-0.13	349 000	-	8	[4]
Piezoresistive	rGO/thermoplastic polyurathane(TPU)	Soft	0.02-1.94	15.2	-	166	[5]
Resistive	Hydrogel/NaOH	Soft	0-3.23	224 000	-	-	[6]
Mechanochromic	inverse opals	-	0-20.4	5.7 nm/%	-	-	[7]
Piezoresistive	Conductive inks	Flexible	0-13.79	-	-	0.05	[1,8]
Electroluminescent	ZnS:Cu/ $SiAlN^3$:Eu^{2+}	Flexible	0-2.4	1.06	-	10	[9]
Piezoresistive	CB/Polyurethane(PU)	Soft	0-0.016	36	-	20	[10]

References

[1] F. Wang, B. Zhu, L. Shu, X. Tao, *Smart Materials and Structures* **2013**, 23, 015001.

[2] Y. Pang, H. Tian, L.-Q. Tao, Y.-x. Li, X. Wang, N.-q. Deng, Y. Yang, T.-l. Ren, *ACS applied materials & interfaces* **2016**, 8 40, 26458.

[3] S. Peng, P. Blanloeuil, S. Wu, C. H. Wang, *Advanced Materials Interfaces* **2018**, 5, 1800403.

[4] Z. Xiao, W. Zhou, N. Zhang, Q. Zhang, X. Xia, X. Gu, Y. Wang, S. Xie, *Small* **2019**, 15, 1804779.

[5] X. Lü, T. Yu, F. Meng, W. Bao, *Advanced Materials Technologies* **2021**, 6, 2100248.
[6] Y. Yang, Y. Yang, Y. Cao, X. Wang, Y. Chen, H. Liu, Y. Gao, J. Wang, C. Liu, W. Wang, J.-K. Yu, D. Wu, *Chemical Engineering Journal* **2021**, 403, 126431.
[7] Y. Cho, S. Y. Lee, L. Ellerthorpe, G. Feng, G. Lin, G. Wu, J. Yin, S. Yang, *Advanced Functional Materials* **2015**, 25, 6041.
[8] a) I. Baldoli, M. Maselli, F. Cecchi, C. Laschi, *Smart Materials and Structures* **2017**, 26, 104011; b) R. Ouckama, D. J. Pearsall, *Journal of Biomechanics* **2011**, 44, 904.
[9] L. Su, Z. Jiang, Z. Tian, H. Wang, H. Wang, Y. Zi, *Nano Energy* **2021**, 79, 105431.
[10] X. Wu, Y. Han, X. Zhang, Z. Zhou, C. Lu, *Advanced Functional Materials* **2016**, 26, 6246.